Region-wide glacier area and mass budgets for the Shaksgam River Basin, Karakoram Mountains, during 2000–2016

WANG Panpan[1], LI Zhongqin[1,2*], XU Chunhai[2], WANG Puyu[2]

[1] College of Geography and Environmental Science, Northwest Normal University, Lanzhou 730070, China;
[2] State Key Laboratory of Cryospheric Sciences/Tianshan Glaciological Station, Northwest Institute of Eco-Environment and Resources, Chinese Academy of Sciences, Lanzhou 730000, China

Abstract: The Karakoram Mountains are well known for their widespread surge-type glaciers and slight glacier mass gains. On the one hand, glaciers are one of the sensitive indicators of climate change, their area and thickness will adjust with climate change. On the other hand, glaciers provide freshwater resources for agricultural irrigation and hydroelectric generation in the downstream areas of the Shaksgam River Basin (SRB) in western China. The shrinkage of glaciers caused by climate change can significantly affect the security and sustainable development of regional water resources. In this study, we analyzed the changes in glacier area from 2000 to 2016 in the SRB using Landsat TM (Thematic Mapper)/ETM+ (Enhanced Mapper Plus)/OLI (Operational Land Imager) images. It is shown that the SRB contained 472 glaciers, with an area of 1840.3 km², in 2016. The glacier area decreased by 0.14%/a since 2000, and the shrinkage of glacier in the southeast, east and south directions were the most, while the northeast, north directions were the least. Debris-covered area accounted for 8.0% of the total glacier area. We estimated elevation and mass changes using the 1 arc-second SRTM (Shuttle Radar Topography Mission) DEM (Digital Elevation Model) (2000) and the resolution of 8 m HMA (High Mountain Asia) DEM (2016). An average thickness of 0.08 (±0.03) m/a, or a slight mass increase of 0.06 (±0.02) m w.e./a has been obtained since 2000. We found thinning was significantly lesser on the clean ice than the debris-covered ice. In addition, the elevation of glacier surface is spatially heterogeneous, showing that the accumulation of mass is dominant in high altitude regions, and the main mass loss is in low altitude regions, excluding the surge-type glacier. For surge-type glaciers, the mass may transfer from the reservoir to the receiving area rapidly when surges, then resulting in an advance of glacier terminus. The main surge mechanism is still unclear, it is worth noting that the surge did not increase the glacier mass in this study.

Keywords: glacier; mass balance; SRTM DEM; HMA DEM; Karakoram Mountains

1 Introduction

Glacier mass balance plays a prominent role in the study of the impact of climate change on glaciers and the response of glaciers to climate change. The local climate determines the supply and loss of mass and energy on the glacier surface and thus determines the mass balance of the glacier. Measurements of the glacier mass balance began in the Alps and Scandinavia in the 1940s. In China, mass-balance measurements began in 1959 with the establishment of the Tianshan Glaciological Station, Chinese Academy of Sciences. To date, the continuous mass balance series, Urumqi Glacier No. 1, Qiyi Glacier and Dongkemadi Glacier, are longer than 20 years in China (Wang et al., 2010; Yao et al., 2012; Wang et al., 2013, 2020). The traditional

*Corresponding author: LI Zhongqin (E-mail: lizq@lzb.ac.cn)
Received 2020-05-13; revised 2020-11-25; accepted 2020-12-19

glaciological method uses stakes or snow pits, which can obtain the mass balance at a single point by measuring the changes in the height of the stakes and the characteristics of the snow pits, and the point values can be extrapolated to the whole glacier to generate the glacier-wide mass balance (Pu et al., 2008). Glaciological mass balance is highly accurate; however, glaciers are usually located in uninhabited high mountains, and measuring stakes or snow pits is time-consuming and laborious, and the cost is too high. Therefore, the number of glaciers monitored by this method is very limited, and traditional methods have limitations in solving the glacier mass balance at the basin scale. With the gradual enrichment of remote sensing data for detecting glacial properties, research on glacier changes through remote sensing data has flourished.

The Karakoram Mountains have a large ice volume, and glacier meltwater provides freshwater for many important inland rivers (e.g., the Yarkant River and Hetian River, both of which are the upper source of the Tarim River), which representing an important part of water resources in western China. According to the fifth report of the IPCC (Intergovernmental Panel on Climate Change), the average surface air temperature of the Earth has increased by 0.89 ℃ over the past 100 years (1901–2012) (IPCC, 2013). Climate warming accelerates the melting of glaciers, which not only threatens the production and life of local people but also affects the rise of sea level (Radić and Hock, 2011; Kääb et al., 2012). In the context of global warming, most of the world's glaciers have suffered mass losses. However, many studies have shown that the glaciers in Karakoram Mountains have experienced a balanced or slightly positive trend over the past decade (Gardelle et al., 2012a; Kääb et al., 2012; Berthier et al., 2019), which may be fostered stable or advancing glacier termini (Bolch et al., 2012; Rankl et al., 2014; Bhambri et al., 2017). This phenomenon is called the "Karakoram Anomaly" (Hewitt, 2005).

Gardelle et al. (2012a) found that glacier mass balance of 0.11 (±0.22) m w.e./a for the Karakoram Mountains (glacier area is 5615.0 km^2) during 2000–2008 using SRTM (Shuttle Radar Topography Mission) DEM (Digital Elevation Model) and SPOT5 stereo image pair data (density: 900 kg/m^3). Kääb et al. (2012) further confirmed that glacier mass balance of –0.06 (±0.04) m w.e./a (glacier area is 21,750.0 km^2) during 2003–2008 by using ICESat laser altimetry (using a density of 900 kg/m^3), and Rankl and Braun (2016) proved that glacier mass balance of –0.08 (±0.10) m w.e./a (glacier area is 1107.0 km^2) for the period 2000–2012 using ice surface elevations of TanDEM-X and SRTM/X-SAR DEM (using a density of 850 kg/m^3). Another study using ICESat (Kääb et al., 2015) and ASTER DEMs from 2000 to 2016 (Brun et al., 2017) has shown that the Karakoram Mountains is located on the western edge of the West Kunlun Mountains, which is a larger mass-balance anomaly, the western Tibetan Plateau. These results indicate that glaciers in the Karakoram Mountains have experienced a stable state although the values slightly different each other.

To overcome the scarcity of existing data sets, we updated the boundary data of glaciers in the SRB (Shaksgam River Basin) from 2000 to 2016. A geodetic method, based on a DEM difference of SRTM and HMA data, was used to determined changes in glacier mass balance during different periods. The function of debris cover in glacier mass changes was understood. Finally, combined with previous studies, discussed and analyzed the characteristics of surge-type glaciers and the climate factors of glacier changes.

2 Study area

The SRB (35°55′–36°49′N, 75°35′–77°30′E), on the northern slope of the Karakoram Mountains, is in western China (Fig. 1). The Shaksgam River, the main river in the SRB, originates from the Karakoram Mountains in Shenglinandaban and flows into the Yarkant River at Cha Hekou. The river course starts from the east-west direction, gradually changes to southeast after 30 km, and finally turns to the east-west direction in the last 40 km (Wang et al., 1989). This area is the upper source area of the Tarim River and is also known as "the Karakoram Corridor". The whole valley runs from southeast to northwest, with an average altitude of approximately 5100 m a.s.l. The world's second-highest peak, Mount Qogir (K2), is its main peak, with an altitude of 8611 m a.s.l.

The SRB is mainly controlled by a continental climate. According to the Chinese Second Glacier Inventory, the SRB contains 491 glaciers (in this paper, some small glaciers are removed) with a total area of 1884.2 km^2. The most densely developed glacier area is Karakoram Mountains, China. Eight glaciers have areas less than 70.0 km^2, which account for 55% of the total glacier area in the study area. The Yengisogat Glacier has an area of 359.1 km^2 and a length of 42 km, and is the largest and longest glacier in China (Liu et al., 2015; Jiang et al., 2020). Due to the high altitude and low air temperature, measurement data are scarce. The Karakoram Mountains have a high altitude and steep terrain. Due to the interception of water and air by the high mountains and the role of storage in the mountains, there is more precipitation in the high-altitude areas than in the low altitude areas, which provides rich mass sources for the formation of glaciers and thus develops the largest and most concentrated glacier group in the middle latitudes (Xu et al., 2016).

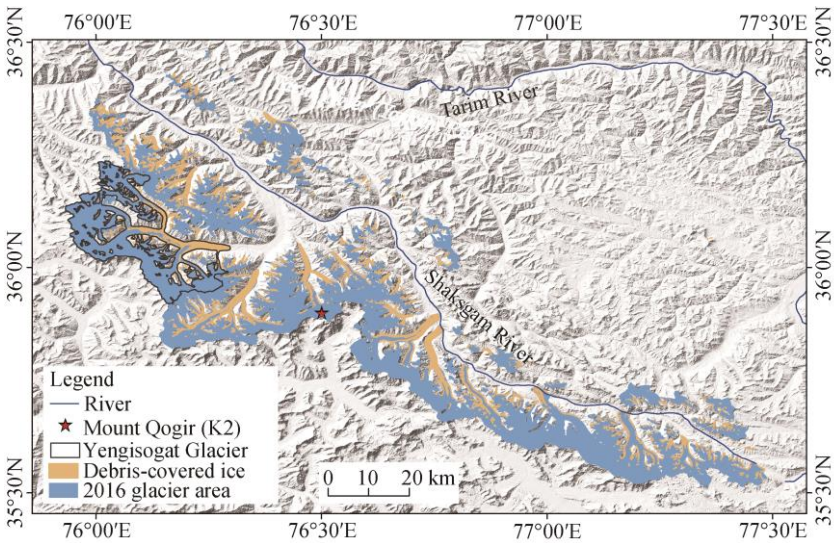

Fig. 1 Location of the study area and distribution of glaciers in 2016. The background map is hillshade of SRTM (Shuttle Radar Topography Mission) DEM (Digital Elevation Model). The debris-covered ice was from Nico et al. (2018).

3 Data

3.1 Landsat data

Landsat images (Table 1) were used to analyze glacier area changes in the SRB, including Landsat TM/ETM+/OLI. Eight Landsat TM/ETM+/OLI images with good quality were used in this study, which were downloaded from the website of USGS (United States Geological Survey; https://earthexplorer.usgs.gov). All scenes are from the USGS and are orthorectified with SRTM and ground control points from the GLS2005 (Global Land Survey 2005) data set, having achieved systematic radiometric and geometric accuracy. Due to the long-time span, high resolution and free download of Landsat data, it has been widely used in glacier remote sensing research (Paul, 2002; Bolch et al., 2010).

3.2 Digital Elevation Models (DEMs)

3.2.1 SRTM DEM

The SRTM acquired interferometric synthetic aperture radar (InSAR) data simultaneously in both

Table 1 Remote sensing images used in this study

Satellite sensor	Period of data	Path/Row	Cloud (%)	Spatial resolution (m)
Landsat TM	29 Aug 1998	148/35	4	30
Landsat TM	4 Sep 2000	148/35	8	30

Landsat ETM+	16 Jul 1999	148/35	13	15/30
Landsat ETM+	16 Jun 2000	148/35	2	15/30
Landsat ETM+	21 Jul 2001	148/35	6	15/30
Landsat ETM+	22 Jun 2002	148/35	3	15/30
Landsat OLI	4 Jul 2015	148/35	3	15/30
Landsat OLI	24 Sep 2016	148/35	6	15/30

the C-band and X-band frequencies from 11 to 22 February 2000 (Farr et al., 2007). Data were acquired between 56 ℃ and 60 ℃, accounting for 80% of the global land surface (Zyl, 2001). The 1 arc-second (30 m) SRTM C-band, with linear vertical absolute height error of less than 16 m, and linear vertical relative height error of less than 10 m (at 90% confidence level). The SRTM DEM can be referred to the glacier surface in the last balance year (1999), with slight seasonal variation (Gardelle et al., 2013). The C-band exhibits some penetration of ice and snow, while the X-band exhibits less penetration. However, because the width of the X-band (50 km) is less than that of the C-band (225 km) (Farr et al., 2007), only 35% of the SRB glaciers are covered by X-band DEM. Low signal, signal-to-noise ratio etc. resulting in voids in the SRTM DEM data, but only 4% of the total glacier area was in the study. Hence, in this study, the 1 arc-second, non-void-filled SRTM C-band DEM was used to estimate the changes in glacier surface elevation after the 1999 ablation period. The data are available free from http://earthexplorer.usgs.gov/.

3.2.2 HMA DEM

The DEMs were generated from high-resolution along-and cross-track stereo images from DigitalGlobe satellites, with a resolution of 8 m, which were collected from 28 January 2002 to 24 November 2016. The HMA DEM is composed of more than 4000 strips with a width of 13.1 km and a length of 17.4 km, which reduces errors and eliminates seams. In this study, six images (100 km×100 km) were collected during 2015–2016. HMA DEM can be referred to the glacier surface in the last balance year (2016), and the data were downloaded free from https://nsidc.org/data/HMA_DEM8m_MOS/versions/1. Although HMA DEM suffers from data voids, otherwise of very high quality (Fig. 2), and the data voids only 5% of the total glacier area.

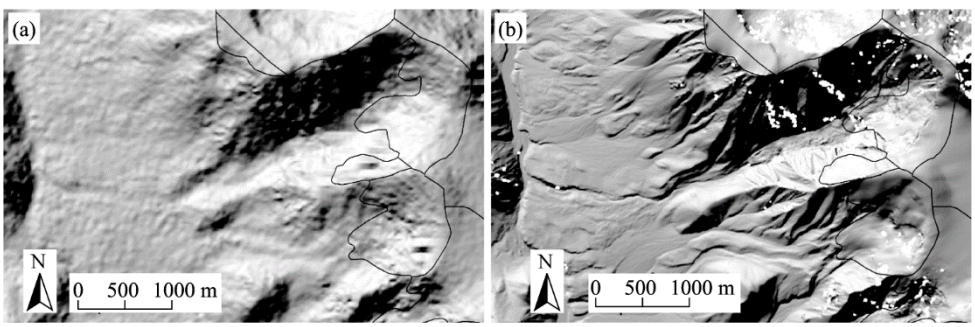

Fig. 2 Resolution comparison of the two DEMs. (a), the 1 arc-second SRTM DEM from 2000; (b), the 8 m HMA (High Mountain Asia) DEM from 2015. The white spots in (b) are voids. The black line cycled areas were glaciers and both pictures were from Paul et al. (2019).

4 Methodology

4.1 Glacier boundary delineation

Information on glacier boundaries is necessary to obtain changes in glacier mass balance. We selected the scenes during the ablation season (from June to September, mainly in August) to minimize the impact of snow cover and comprehensively considered the time, cloud proportion (Table 1). Seasonal snow and clouds can be distinguished by comparing images of the glacier body from neighboring years.

Because of its simplicity and accuracy, the band ratio is the most suitable method to extract

glacier boundary (Albert, 2002; Paul et al., 2015). We use the method of band ratio threshold (TM3/TM5 for TM/ETM+ and TM4/TM6 for OLI), with a threshold of 1.9 chosen for this task. The principle is to divide the surface object into glacierized and non-glacierized area by using the strong reflectivity of glaciers in the visible light band and the strong absorption in the near-infrared band. This method may mistake proglacial lakes for glaciers (Pan et al., 2012). Visual interpretation can easily correct this error. The surfaces of glaciers in the study area are covered by debris and supraglacial boulders, and the identification of these features is time-consuming and important work in later editing. There are several principles for distinguishing debris-covered glaciers. For example, Käab (2005) suggested that areas with slopes lower than the threshold (23 °) and directly connected to clean ice can be considered ice covered by debris. The colour of the surface moraine on the glacier is different from that of the debris on the outer edge of the glacier. The supraglacial boulders throughout a glacier tongue have the same spectral characteristics. With the increase in air temperature, the shape of the glacier tongue obviously decreases, which can be identified. Therefore, the above principles can be used to identify supraglacial boulders and debris-covered ice. At the same time, the process of extracting glacier information also refers to the second Chinese glacier inventory (http://westdc.westgis.ac.cn/) and Google Earth.

Although we have made extensive efforts to improve the accuracy of extracted glacier boundaries, errors still exist for various reasons. A certain degree of error assessment is needed. In this paper, the method proposed by Jin et al. (2005) is used to evaluate the error of the glacier boundaries. First, the buffer zone of the glacier boundary extracted from TM, ETM+ and OLI images are analyzed (taking half of the resolution of the remote sensing image as the buffer distance; thus, TM, ETM+ and OLI images have a buffer distance of 15 m). Then, the glacier area in the buffer zone is differentiated from the glacier area extracted from the original image, and the ratio between the result and the latter is the uncertainty of the glacier area extraction. The results showed that the uncertainty values of the extracted glacier boundaries in 2000 and 2016 were ±3.72% and ±3.54%, respectively, which were both within the range of previous research results (He and Yang, 2014).

4.2 Geodetic mass balance calculations

We use the geodetic method to obtain the glacier surface elevation changes by comparing the DEM data from different periods and then to estimate the glacier mass balance by combining the area and density of glaciers (Thibert et al., 2008; Fischer, 2011).

$$B=\frac{\rho}{S_g}\sum_{i=1}^{M}\Delta h_i S_P\,, \tag{1}$$

where B is the glacier mass balance (m w.e.); ρ is the ice density (kg/m^3); S_g is the glacier area (km^2); M is the number of pixels contained in the glacier boundary; Δh_i is the glacier surface elevation difference (m); and S_p is the pixel size (m), that is, the spatial resolution of the DEM data.

4.3 Co-registration and correction of DEMs

Due to the differences in DEM acquisition, geodetic reference planes and processing methods, horizontal and vertical shifts might exist between the SRTM DEM and the HMA DEM. Any small horizontal shift will cause obvious DEM elevation errors in the mountain area. However, before estimating the elevation changes of the glacier surface, the relative registration of each DEM data is needed. Here, we used the method proposed by Nuth and Käab (2011). Research shows that there is a cosine-curved obvious relationship between elevation difference, aspect and slope (Käab, 2005) (Fig. 3a), based on the relationship relative vertical and horizontal distortions between the SRTM DEM and HMA DEM was corrected statistically (Nuth and Käab, 2011). Based on the SRTM DEM, the spatial resolution of the HMA DEM was resampled to 30 m. Under the support of ArcGIS 10.2.2 software, a difference map was built with the SRTM C-band DEM and HMA DEM. On the basis of statistical analysis, 5% and 95% quantile thresholds are used to eliminate outliers DEM edges and near data gaps (Pieczonka and Bolch, 2015). Based on cosine fitting, we obtained the translation vector, and then the HMA DEM was moved to achieve

image registration. The calculation is as follows (Eqs. 2–6). In addition, based on the relationship between the elevation difference and the maximum curvature in non-glacier regions (Fig. 3b), the deviation, caused by the different spatial resolution of the two datasets, were refined for both glacier and non-glacier regions (Gardelle et al., 2012b). Before adjustment, the average elevation difference and standard deviation of the non-glacier regions were –19.83 and 14.91 m respectively. After these adjustments, the elevation difference in the non-glacier regions was focused on the average elevation difference at –0.38 m, and the standard deviation was reduced to 11.8 m. After these corrections, the non-glacier regions had stabilized, which makes the DEMs suitable for estimating the change of glacier mass balance.

$$\frac{dh}{\tan(\alpha)} = a \times \cos(b - \varphi) + c, \tag{2}$$

$$c = \frac{\overline{dh}}{\tan(\overline{\alpha})}, \tag{3}$$

where dh is the individual elevation difference (m); α and φ represent the slope and aspect of the pixel (°), respectively; $\overline{dh}$ is the overall elevation bias between the SRTM DEM and HMA DEM (m), representing the vertical offset; a is the magnitude of the horizontal shift (m); b is the direction of the shift vector (°); c is the mean bias between the DEMs divided by the mean slope tangent (m), and $\overline{\alpha}$ is the average slope of the DEM data (°).

The offset in the x (m), y (m) and z (m) directions between the two DEMs can be calculated by the following formulas:

$$x = a \times \sin(b), \tag{4}$$

$$y = a \times \cos(b), \tag{5}$$

$$z = c \times \tan(\overline{\alpha}), \tag{6}$$

where a, b and c can be obtained by cosine fitting.

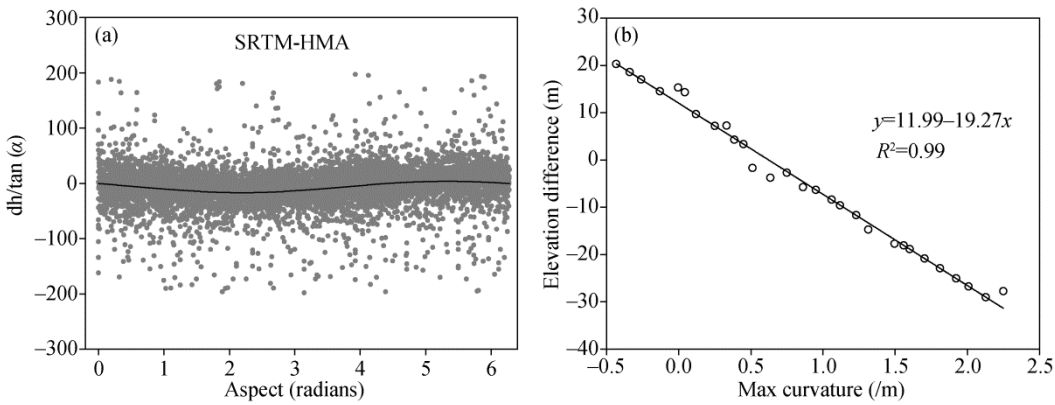

Fig. 3 (a) Scatter plot of aspect vs slope for the standardized elevation differences for non-glacier areas. (b) Relationship between elevation difference and maximum curvature in the non-glacier areas of SRB (Shaksgam River Basin).

4.4 Uncertainty assessment

4.4.1 Evaluation of elevation change uncertainty

The root mean square error or standard deviation of the elevation residuals between different DEMs in the area away from a glacier can estimate the uncertainty of the elevation changes (Bolch et al., 2011).

$$E_\sigma = \frac{\mathrm{SD}_{\text{no glac}}}{\sqrt{N}}, \tag{7}$$

$$E = \sqrt{E_m^2 + E_\sigma^2}, \tag{8}$$

where E_σ is the average elevation bias of off glaciers (m); $\mathrm{SD}_{\text{no glac}}$ is the standard deviation in the non-glacial areas (m); N is the number of measurement points; E_m is the average elevation difference in non-glacier areas (m); and E is the error of elevation change (m).

In order to calculate E_σ for a reasonable number of pixels near the glacier, we only used the pixels in the 5 km buffer zone around the glacier. Note that the DEM exhibits strong spatial autocorrelation in the elevation values of adjacent grids. To reduce the influence of autocorrelation, a decorrelation length based on the spatial resolution is suggested. For DEMs with a spatial resolution of 30 m, 600 m is suitable as the decorrelation length (Koblet et al., 2010).

Table 2 Statistical results of the vertical error before and after the adjustment of the HMA (High Mountain Asia) and SRTM (Shuttle Radar Topography Mission) DEMs (Digital Elevation Models) in non-glacier areas

Before co-registration		After co-registration		N	E_σ (m)	E (m)
E_m (m)	$\mathrm{SD}_{\text{no glac}}$ (m)	E_m (m)	$\mathrm{SD}_{\text{no glac}}$			
–19.83	14.91	–0.38	11.80	6960	0.14	0.41

Note: E_m, average elevation difference in non-glacier areas; $\mathrm{SD}_{\text{no glac}}$, standard deviation in the non-glacier areas; N, number of measurement points; E_σ, average elevation bias of off glaciers; E, error of elevation change.

4.4.2 Effect of SRTM penetration

The SRTM C-band (5.7 GHz) exhibits some penetration of ice and snow with a penetration depth between 1 and 10 m (Rignot et al., 2001). The penetration of the SRTM X-band (9.7 GHz) is expected to be low compared to that of the C-band (a hypothesis that still needs to be confirmed (Ulaby et al., 1986), we consider the elevation difference (SRTM C-band−SRTM X-band) to be the first approximation of C-band radar penetration over glaciers (Gardelle et al., 2012b). Here, we estimate this penetration by differencing the SRTM C-band and X-band DEMs. The X-band and C-band are acquired simultaneously. There is no elevation change caused by ablation or accumulation (Gardelle et al., 2012b, 2013; Shangguan et al., 2015). Before estimating the penetration depth of the SRTM C-band, the SRTM X DEM and C DEM were co-registered and corrected. The final mean SRTM C-band penetration depth over the SRB was approximately 2.8 m, which is consistent with the results of Gardelle et al. (2013), who reported a penetration depth of 3.4 m.

4.4.3 Density assumption error

The conversion from ice volume to mass is an important part when estimating glacier mass changes using the geodetic method (Huss, 2013). The glacier density must be considered to convert glacier elevation change to a mass balance change. Fresh snow, firn and ice exhibit large differences in density, and the density of glaciers varies, ranging from 100 to 917 kg/m^3 (Fischer, 2011). The density parameter value will produce 5%–6% uncertainty in the glacier scale mass balance estimation results (Elsberg et al., 2001). In the Karakoram Mountains, it is assumed that the parameters used to convert the glacier elevation change into mass changes follow Sorge's law (Bader, 1954), that is, glacier density remains constant in the vertical direction, 900 kg/m^3 is used as the density conversion parameter, and the estimated mass balance was 0.11 (±0.22) m w.e./a during 1999–2008. If the glacial density in the accumulation zone is assumed to be 600 kg/m^3, the mass balance drops to 0.05 (±0.16) m w.e./a, and both extreme density scenarios did not change the result of the proximity of the glacier area. In this study, a density of 850 kg/m^3, with an uncertainty of 60 kg/m^3, was used as the volume-to-mass conversion parameter.

4.4.4 Accuracy of the glacier boundary

The uncertainty of the glacier area refers to the error caused by the differences in S_g and M in Equation 1, which is used to estimate the mass balance. To reduce this error, when calculating the changes in glacier volume, the maximum glacier area after the fusion of two periods can be taken;

when calculating the mass balance of glaciers, the union value of the glacier boundary from two periods can be taken (Gardelle et al., 2012b, 2013; Pieczonka et al., 2013). We finally obtained glacier areas in 2000 and 2016 of 1884.2 and 1840.3 km^2, respectively.

4.4.5 Uncertainty of mass balance

The final mass balance uncertainty was determined using the estimated uncertainties of glacier area and elevation changes, and the glacier density uncertainty was 60 kg/m^3:

$$E_{\mathrm{MB}} = \sqrt{\left(\frac{\Delta h}{t} \times \frac{\Delta \rho}{\rho_w}\right)^2 + \left(\frac{E}{t} \times \frac{\rho_i}{\rho_w}\right)^2}, \tag{9}$$

where E_{MB} is the uncertainty of mass balance (m w.e./a); t is the observation period; ρ_i is the ice density (850 kg/m^3); $\Delta\rho$ is the ice density uncertainty (60 kg/m^3); and ρ_w is the water density (999.92 kg/m^3) (Pieczonka et al., 2013).

5 Results

5.1 Area changes

There were 472 glaciers with a total area of 1840.3 km^2 in 2016 in the SRB (Fig. 4). In terms of area, large glaciers (≥1 km^2, occupy 94.3% of the total area) are dominant, while small glaciers (<1.0 km^2, occupy 70.6% of the total number) are dominant in number (Fig. 4a). The glacier surface slope in the SRB is approximately in the 16 °–34 ° range, accounting for 95.6% of the total glacier area. Glaciers having a north, northeast, northwest or east aspects account for 63.2% of the total area. The shrank of the glacier on the southeast, east and south aspects were the most, while those on the west, northeast and north aspects were the least (Fig. 4b).

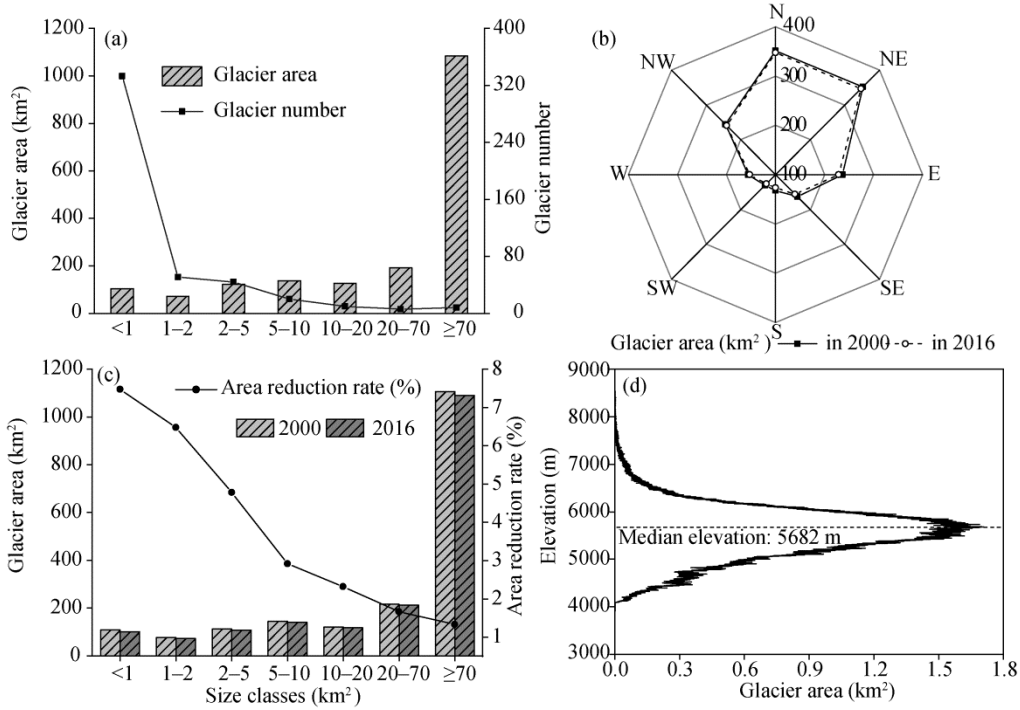

Fig. 4 Glacier distribution and change in the SRB. (a), area and number of 2016 glaciers in different size classes; (b), distribution of glacier area in different slope directions in 2000 and 2016; (c), the change of glacier area and area reduction rate under different size classes from 2000 to 2016; (d), the distribution of glacier area with elevation in 2016.

The glaciers were significantly debris covered in the SRB and the distribution of debris-covered glaciers is shown in Figure 1. The total debris-covered area was 146.5 km^2.

Among all debris-covered glaciers, there were 20 glaciers with debris-covered areas larger than 1.0 km^2. Yengisogat Glacier has the most debris cover in the SRB (32.9 km^2, about 9.3% of its area). About 86.2% of the debris-covered area is in the 4200 and 5200 m altitude range, 10.7% is higher than 5200 m, and only 3.1% is below 4200 m.

Comparing the area of glaciers in 2000 with that in 2016, the reduction in glacier area was 43.9 km^2, with an annual average shrinkage rate of 0.14%/a. Small glaciers shrink significantly, however, the area loss of large glaciers is dominant in absolute area loss (Fig. 4c). Approximately 91.5% of the total glacier area is found from 4400 to 6300 m, while only 1.6% is below 4400 m, and 6.2% above 6300 m. The median elevation is about 5682 m (Fig. 4d). The glacier topography analysis shows that the glacier area below 4000 m had disappeared completely, with an area of 0.3 km^2. Glaciers at low altitudes disappeared, and glaciers at high altitudes change very little and without disintegration, causing the decrease of the total number of glaciers. Glaciers in the SRB have experienced weakening area shrinkage from 2000 to 2016.

5.2 Elevation and mass changes

The glaciers in the SRB appear to show a weak surface thickening from 2000 to 2016. Glaciers, with an area of 1862.3 km^2 (the union of the 2000 and 2016 glacier extents), experienced a thickening of 1.21 (±0.41) m (0.08 (±0.03) m/a). Using 850 (±60) kg/m^3 as the density parameter, glacier mass gain of 0.06 (±0.02) m w.e./a. The distribution of glacier surface mass is uneven (Fig. 5), which shows that the accumulation of mass is dominant in high altitude regions, and the loss of mass in low altitude regions (excluding the surge glacier). Yengisogat Glacier is typical. There are obvious glacier thickening phenomena in the upper reaches of the North ice flow (A in Fig. 5a), the upper reaches of the northwest ice flow (B in Fig. 5a), and the middle part of the main stream (C in Fig. 5a).

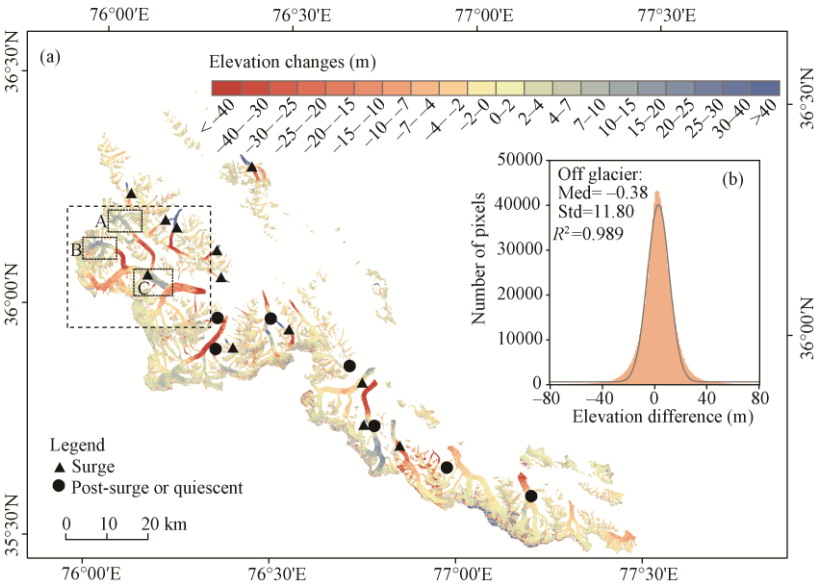

Fig. 5 Changes in glacier surface elevation in the SRB from 2000 to 2016. The glacier boundaries are based on the union of the 2000 and 2016 glacier area. These surge-type glacier and post-surge or quiescent during 1999–2011 were reported by Gardelle et al. (2012a, 2013).

6 Discussion

6.1 Comparison with previous study

Previous studies agreed that the mass balance of glaciers in the Karakoram Mountains has maintained a weak increase or stable state since 2000 (Table. 3). Based on SRTM and SPOT5 DEMs, a thickening of 0.12 (±0.19) m/a was found from 2000 to 2011 by Gardelle et al. (2013). Whereas a thinning of 0.09 (±0.12) m/a between 2000 and 2012 was reported over the Karakoram

by Rankl and Braun (2016), using Tan DEM_X and SRTM/X_ASR. And a thinning of 0.07 (±0.04) m/a (2003–2008) was found in the Karakoram by Kääb et al. (2012), using SRTM and ICESat. In this study, SRTM and HMA DEMs acquisitions a mean thickening of 0.08 (±0.03) m/a between 2000 and 2016. This positive trend agrees with the results of Gardelle et al. (2013) but has slight differences from the results (a weak negative trend) of Kääb et al. (2012), and Rankl and Braun (2016). Different estimates of SRTM C-band penetration result in different thicknesses with those determined by Kääb et al. (2012). A mean SRTM C-band penetration of 2.4 (±0.3) m was used for the Karakoram Mountains (Kääb et al., 2012), less than 3.0 m (snow and ice), 8.0 m (accumulation areas) and an average penetration of 3.4 m in the central Karakoram Mountains (Gardelle et al., 2012a, 2013) and 2.8 m assumed in this study. The Karakoram Mountains is located at the west end of the Himalayan arc, stretching for thousands of kilometers, containing around 19,950.0 km^2 of glaciers (Cogley, 2011). The characteristics of glaciers in the eastern, western and central Karakoram Mountains are different. The study area of Gardelle et al. (2013) is mainly concentrated in the central Karakoram, while the study area of Kääb et al. (2012) covers the whole Karakoram Mountains, our study area is mainly located at the eastern and central Karakoram Mountains. In addition, the differences in DEMs, the density of snow ice and glacier boundaries may explain part of these discrepancies. Previous studies estimated an average penetration depth of 2.7 m in the Karakoram Mountains (Zhou et al., 2017), 2.8 m in West Kunlun Mountains, 1.9 m in Pamir (Lin et al., 2017), 3.5 m in the Hindu Kush and 2.0–3.0 m in the Karakoram Mountains (Chen et al., 2018). In this study, the penetration depth was 2.8 m, in agreement with previous studies, which was considered acceptable and suitable for estimating glacier elevation changes in the SRB. However, these studies suggested that the average changes in glacier surface elevation of the Karakoram Mountains are certainly relatively small, even the glaciers have experienced a stable status in the Karakoram Mountains.

Table 3 Comparison of mass balance budgets in this study and others

Region	Study period	Elevation change (m/a)	Mass balance (m w.e./a)	Reference
Karakoram Mountains	2003–2008	–0.07（±0.04）	–0.06 (±0.04)	Kääb et al. (2012)
Karakoram Mountains	2003–2009	–0.12 (±0.15)	-	Gardner et al. (2013)
Central Karakoram	2000–2010	0.12 (±0.19)	0.10 (±0.16)	Gardelle et al. (2013)
Central Karakoram	2000–2012	–0.09 (±0.12)	–0.08 (±0.10)	Rankl and Braun (2016)
Central Karakoram	1999–2008	-	0.11 (±0.22)	Gardelle et al. (2012a)
SRB	2000–2016	0.08 (±0.03)	0.06 (±0.02)	This study

Note: - indicates no data available.

6.2 Debris-covered ice and clean ice

The debris-covered areas account for about 8.0% of the total glacier (Fig. 6a). Ice cliffs, heterogeneous debris cover and supraglacial lakes could be the contributing factors to the complexity of the mass-loss patterns of debris-covered tongues (Pellicciotti et al., 2015). Although it is generally believed that a thick debris cover will act as a protective layer for glaciers due to its insulation (Benn et al., 2000), previous studies have reported that it will accelerate when the thickness of debris cover is smaller than a critical value (Ye et al., 2015; Zhang et al., 2016). In this study, the debris cover has a positive influence on the ablation, and we found that melt was noticeably smaller on the clean ice than the debris-covered ice in the altitude 4000–5900 m, during 2000–2016 (–0.63 (±0.03) vs 0.13 (±0.03) m/a) (Fig. 6b). Previous studies have found similar results in the Karakoram Mountains (Gardelle et al., 2012a), the eastern Pamir (Zhang et al., 2016), and the central Nyainqentanglha Range (Wu et al., 2019).

6.3 Surge-type glaciers

According to previous studies, at least 12 places surged in this basin (Fig. 5). Among the 12 places, most surges occurred between 2000 and 2016 (Quincey et al., 2015; Bhambri et al., 2017), and one of them (C position in Figure 5a) occurred during 2011–2016. During 1999–2011, the C

position was defined with dashed black box in a post-surge or quiescent phase. Here, we found that an obvious thickening occurred at the C position, at the same time, there was obvious thinning in the upper reaches (below the A and B in Figure 5a), which is consistent with the characteristics of surge-type glaciers. In this study, we can't determine the specific time of the glacier surged here. However, according to the reported study, it is indicated that the C position (Fig. 5) of Yengisogat Glacier has a faster movement velocity of 900 m/a from June to August 2012. Then, the glacier movement velocity decreased rapidly, that is, from June to August 2012, it may be at the peak of the surge phase (Quincey et al., 2015).

Most of the glaciers either have stable termini locations or have been advancing, partly as a result of increased local precipitation (Janes et al., 2012) and partly due to glacier surging (Paul, 2015) in the Karakoram Mountains. Here, the glacier surging did not increase the glacier mass. Generally, the rapid transfer of mass to the receiving area resulted in an advance of the glacier termini, but it was not always. Although some characteristics of the Karakoram glacier surges are similar to thermally controlled surges of other places (such as Svalbard), the main surge mechanism is still unclear (Quincey et al., 2015).

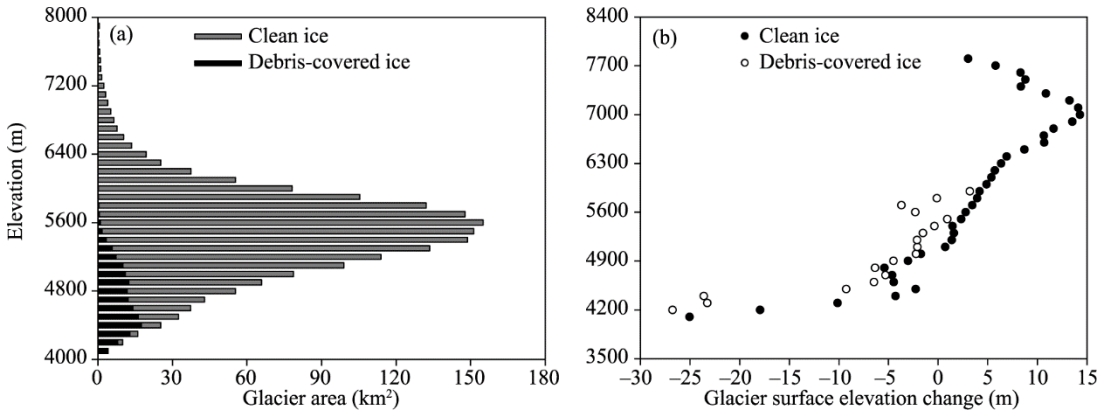

Fig. 6 Distribution of glacier area in 2016 (a) and glacier surface elevation changes during 2000–2016 (b) at 100-m intervals by elevation in the SRB for debris-covered ice and clean ice

6.4 Analysis of the factors of glacier anomaly

Glaciers are a comprehensive product of climate, topography and other factors. Since the terrain has not changed in recent decades or even hundreds of years, glaciers are sensitive to climate change (Shi, 2000). Some potential explanations, such as cloud cover, precipitation and temperature can be found in the current studies, which may be driving factors of the Karakoram glacier changes. Based on the global meteorological reanalysis data and meteorological station data, Forsythe et al. (2015) and Bashir et al. (2017) have reported that an increase of cloudiness in the Karakoram Mountains. The increase of cloud cover may reduce the incoming shortwave radiation (Forsythe et al., 2015). However, incoming shortwave radiation is generally considered to be the main energy source of glacier mass changes (Forsythe et al., 2015). In addition, previous studies have reported that increased cloud cover leads to increase in precipitation (Forsythe et al., 2015; Bashir et al., 2017). The climate of Karakoram is mainly influenced by westerly circulation and Tibetan anticyclone (Archer and Fowler, 2004). Cannon et al. (2015) reported that the frequency and intensity of such precipitation by westerlies-dominated have increased in recent years, which seems to lead to a slight increase in winter snowfall in Karakoram (Norris et al., 2019). In turn, precipitation change is considered to be a powerful control on glacier mass balance in the Karakoram Mountains (Kapnick et al., 2014; Forsythe et al., 2017). Moreover, in recent decades, summer cooling has been a particularly important driving factor for the mass balance of glaciers in the Karakoram Mountains (Fowler et al., 2010; Forsythe et al., 2017). It is worth noting that the tree-ring chronology did not provide any evidence that the temperature of the Karakoram Mountains is not consistent with the rest regions in High Mountain Asia.

7 Conclusions

This paper takes the glaciers in the SRB as the research object, and the glacier boundaries in 2000 and 2016 were extracted according to Landsat TM/ETM+/OLI images. Based on HMA DEM and SRTM DEM data, changes in surface elevation and mass balance in this study have been estimated from 2000 to 2016.

We found that the SRB contained 472 glaciers, with a total glacier area of 1840.3 km^2 in 2016. The reduction in glacier area was 43.9 km^2 with an annual average shrinkage rate of 0.14%/a, and glacier area mainly decreased in the southeast, east and south directions, during 2000–2016. Compared with the melt of mountain glaciers in western China, even global, the glaciers in the SRB have experienced a slight shrinkage. In addition, the debris-covered area was 146.5 km^2, accounting for about 8.0% of the total area.

The glacier thickness showed a weak increasing trend, with a thickening value of 0.08 (±0.03) m/a, or 0.06 (±0.02) m w.e./a. The thinning value was significantly greater on the debris-covered ice than the clean ice in the altitude 4000–5900 m, between 2000 and 2016 in the SRB (–0.63 (±0.03) vs 0.13 (±0.03) m/a). Research result shows that the glacier mass was rapidly transferring from the reservoir to the receiving area, resulting in an advance of the glacier termini, but not always.

Acknowledgements

This work was supported by the Second Tibetan Plateau Scientific Expedition and Research Program (2019QZKK0201), the Strategic Priority Research Program of Chinese Academy of Sciences (XDA20060201, XDA20020102), the National Natural Science Foundation of China (41761134093, 41771077, 42001067), the State Key Laboratory of Cryosphere Science founding (SKLCS-ZZ-2019), and the National Science and Technology Basic Resources Survey Program of China (2019FY100202).

References

Albert T H. 2002. Evaluation of remote sensing techniques for ice-area classification applied to the tropical Quelccaya Ice Cap, Peru. Polar Geography, 26(3): 210–226.

Archer D R, Fowler H J. 2004. Spatial and temporal variations in precipitation in the Upper Indus Basin, global teleconnections and hydrological implications. Hydrology and Earth System Sciences, 8(1): 47–61.

Bader H. 1954. Sorge's law of densification of snow on high polar glaciers. Journal of Glaciology, 2(15): 319–323.

Bashir F, Zeng X B, Gupta H, et al. 2017. A hydrometeorological perspective on the Karakoram anomaly using unique valley-based synoptic weather observations. Geophysical Research Letters, 44(20): 10470–10478.

Benn D I, Lehmkuhl F. 2000. Mass balance and equilibrium-line altitudes of glaciers in high-mountain environments. Quaternary International, 65–66: 15–29.

Berthier E, Brun F. 2019. Karakoram geodetic glacier mass balances between 2008 and 2016: persistence of the anomaly and influence of a large rock avalanche on Siachen Glacier. Journal of Glaciology, 65(251): 494–507.

Bhambri R, Hewitt K, Kawishwar P, et al. 2017. Surge-type and surge-modified glaciers in the Karakoram. Scientific Reports, 7(1): 15391, doi: 10.1038/s41598-017-15473-8.

Bolch T, Menounos B, Wheate R, et al. 2010. Landsat-based inventory of glaciers in western Canada, 1985–2005. Remote Sensing of Environment, 114(1): 127–137.

Bolch T, Pieczonka T, Benn D I. 2011. Multi-decadal mass loss of glaciers in the Everest area (Nepal Himalaya) derived from stereo imagery. The Cryosphere, 5: 349–358.

Bolch T, KulkarniA, Kääb A, et al. 2012. The state and fate of Himalayan glaciers. Science, 336(6079): 310–314.

Brun F, Berthier E, Wagnon P, et al. 2017. A spatially resolved estimate of High Mountain Asia glacier mass balances from 2000 to 2016. Nature Geoscience, 10(9): 668–658.

Cannon F, Carvalho L M V, Jones C, et al. 2015. Multi-annual variations in winter westerly disturbance activity affecting the Himalaya. Climate Dynamics, 44(1–2): 441–455.

Chen A A, Li Zhe, He J Q, et al. 2018. Study of penetration depth for the SRTM C-band DEM in the glacier area over the High Mountain Asia. Journal of Glaciology and Geocryology, 40(1): 26–37.

Cogley G J. 2011. Present and future states of Himalaya and Karakoram glaciers. Annals of Glaciology, 52(59): 69–73.

Elsberg D H, Harrison W D, Echelmeyer K A, et al. 2001. Quantifying the effects of climate and surface change on glacier mass

balance. Journal of Glaciology, 47(159): 649–658.
Farr T G, Rosen P A, Caro E, et al. 2007. The shuttle radar topography mission. Reviews of Geophysics, 45(2): 361.
Fischer A. 2011. Comparision of direct and geodetic mass balances on a multi-annual time scale. Cryosphere Discussions, 5(1): 565–604.
Forsythe N, Hardy A J, Fowler H J, et al. 2015. A detailed cloud fraction climatology of the upper indus basin and its implications for near-surface air temperature. Journal of Climate, 28(9), 3537–3556.
Forsythe N, Fowler H J, Li X F, et al. 2017. Karakoram temperature and glacial melt driven by regional atmospheric circulation variability. Nature Climate Change, 7: 664–670.
Fowler H J, Archer D R. 2010. Conflicting signals of climatic change in the Upper Indus Basin. Journal of Climate, 19(17): 4276–4293.
Gardelle J, Berthier E, Arnaud Y. 2012a. Slight mass gain of Karakoram glaciers in the early twenty-first century. Nature Geoscience, 5(5): 322–325.
Gardelle J, Berthier E, Arnaud Y. 2012b. Impact of resolution and radar penetration on glacier elevation changes computed from DEM differencing. Journal of Glaciology, 58(208): 419–422.
Gardelle J, Berthier E, Arnaud Y, et al. 2013. Region-wide glacier mass balances over the Pamir–Karakoram–Himalaya during 1999–2011. The Cryosphere, 7(4): 1263–1286.
Gardner A S, Moholdt G, Cogley J G, et al. 2013. A reconciled estimate of glacier contributions to sea level rise: 2003 to 2009. Science, 340(6134): 852–857.
He Y, Yang T. 2014. Climate variation and glacier response in the Bogda region, Tianshan Mountains. Progress in Geography, 33(10): 1387–1396. (in Chinese)
Hewitt K. 2005. The Karakoram Anomaly? Glacier expansion and the 'Elevation Effect', Karakoram Himalaya. Mountain Research Development, 25(4): 332–340.
Huss M. 2013. Density assumptions for converting geodetic glacier volume change to mass change. The Cryosphere, 7(7): 877–887.
IPCC (ntergovernmental Panel on Climate Change). 2013. Climate Change 2013: The Physical Science Basis. Contribution of Working Group I to the Fifth Assessment Report of the Intergovernmental Panel on Climate Change. Cambridge: Cambridge University Press, 1535.
Janes T J, Bush A B G. 2012. The role of atmospheric dynamics and climate change on the possible fate of glaciers in the Karakoram. Journal of Climate, 25(23): 8308–8327.
Jiang Z L, Wang L, Zhang Z, et al. 2020. Surface elevation changes of Yengisogat Glacier between 2000 and 2014. Arid Land Geography, 43(1): 12–19. (in Chinese)
Jin R, Li X, Che T, et al. 2005. Glacier area changes in the Pumqu river basin, Tibetan Plateau, between the 1970s and 2001. Journal of Glaciology, 51(175): 607–610.
Kääb A. 2005. Remote Sensing of Mountain Glaciers and Permafrost Creep. Switzerland: Schriftenreihe Physische Geographie, 48: 266.
Kääb A, Berthier E, Nuth C, et al. 2012. Contrasting patterns of early twenty-first-century glacier mass change in the Himalayas. Nature, 488(7412): 495–498.
Kääb A, Treichler D, Nuth C, et al. 2015. Brief communication: contending estimates of 2003–2008 glacier mass balance over the Pamir–Karakoram–Himalaya. Cryosphere, 9: 557–564.
Kapnick S B, Delworth T L, Ashfaq M, et al. 2014. Snowfall less sensitive to warming in Karakoram than in Himalayas due to a unique seasonal cycle. Nature Geoscience, 7(11): 834–840.
Koblet T, Gartner-Roer I, Zemp M, et al. 2010. Reanalysis of multi-temporal aerial images of Storglaciären, Sweden (1959-99)–Part 1: determination of length, area, and volume changes. The Cryosphere, 4: 333–343.
Lin H, Li G, Cuo L, et al. 2017. A decreasing glacier mass balance gradient from the edge of the Upper Tarim Basin to the Karakoram during 2000–2014. Scientific Reports, 7(1): 6712, doi: 10.1038/s41598-017-07133-8
Liu S Y, Yao X J, Guo W Q, et al. 2015. The contemporary glaciers in China based on the Second Chinese Glacier Inventory. Acta Geographica Sinica, 70(1): 3–16. (in Chinese)
Nico M, Tobias B, Philipp R., et al. 2018. A consistent glacier inventory for Karakoram and Pamir derived from Landsat data: distribution of debris cover and mapping challenges. Earth System Science Data, 10(4): 1807–1827.
Norris J, Carvalho L M V, Jones C, et al. 2019. Deciphering the contrasting climatic trends between the central Himalaya and Karakoram with 36 years of WRF simulations. Climate Dynamics, 52(1–2): 159–180.
Nuth C, Kääb A. 2011. Co-registration and bias corrections of satellite elevation data sets for quantifying glacier thickness change. The Cryosphere, 5(1): 271–290.
Pan B T, Zhang G L, Wang J, et al. 2012. Glacier changes from 1966–2009 in the Gongga Mountains, on the south-eastern margin of the Qinghai-Tibetan Plateau and their climatic forcing. The Cryosphere, 6(5): 1087–1101.
Paul F. 2002. Changes in glacier area in Tyrol, Austria, between 1969 and 1992 derived from Landsat 5 Thematic Mapper and Austrian Glacier Inventory data. International Journal of Remote Sensing, 23(4): 787–799.

Paul F. 2015. Revealing glacier flow and surge dynamics from animated satellite image sequences: Examples from the Karakoram. The Cryosphere, 9(2): 2597–2623.

Paul F, Bolch T, Kääb A, et al. 2015. The glaciers climate change initiative: Methods for creating glacier area, elevation change and velocity products. Remote Sensing of Environment, 162: 408–426.

Paul F. 2019. Repeat glacier collapses and surges in the Amney Machen Mountain Range, Tibet, possibly triggered by a developing rock-slope instability. Remote Sensing, 11(6): 708–725.

Pellicciotti F, Stephan C, Miles E, et al. 2015. Mass-balance changes of the debris-covered glaciers in the Langtang Himal, Nepal, between 1974 to 1999. Journal of Glaciology, 61(226): 373–386.

Pieczonka T, Bolch T, Wei J, et al. 2013. Heterogeneous mass loss of glaciers in the Aksu-Tarim Catchment (Central Tien Shan) revealed by 1976 KH-9 Hexagon and 2009 SPOT-5 stereo imagery. Remote Sensing of Environment, 130: 233–244.

Pieczonka T, Bolch T. 2015. Region-wide glacier mass budgets and area changes for the Central Tien Shan between ~1975 and 1999 using Hexagon KH-9 imagery. Global and Planetary Change, 128: 1–13.

Pu J, Yao T, Yang M, et al. 2008. Rapid decrease of mass balance observed in the Xiao (Lesser) Dongkemadi Glacier, in the central Tibetan Plateau. Hydrological Process, 22: 2953–2958.

Quincey D J, Glasser N F, Cook S J, et al. 2015. Heterogeneity in Karakoram glacier surges. Journal of Geophysical Research: Earth Surface, 120(7): 1288–1300.

Radić V, Hock R. 2011. Regionally differentiated contribution of mountain glaciers and ice caps to future sea-level rise. Nature Geoscience, 4(2): 91–94.

Rankl M, Kienholz C, Braun M. 2014. Glacier changes in the Karakoram region mapped by multimission satellite imagery. The Cryosphere, 8(3): 977–989.

Rankl M, Braun M H. 2016. Glacier elevation and mass changes over the central Karakoram region estimated from TanDEM-X and SRTM/X-SAR digital elevation models. Annals of Glaciology, 57(71): 273–281.

Rignot E, Echelmeyer K, Krabill W. 2001. Penetration depth of interferometric synthetic-aperture radar signals in snow and ice. Geophysical Research Letters, 28(18): 3501–3504.

Shangguan D H, Bolch T, Ding Y J, et al. 2015. Mass changes of Southern and Northern Inylchek Glacier, Central Tian Shan, Kyrgyzstan, during ~1975 and 2007 derived from remote sensing data. The Cryosphere, 9(2): 703–717.

Shi Y. 2000. Glacier and their Environments in China: The Present, Past And Future. Beijing: Science Press, 35–37. (in Chinese)

Thibert E, Blanc R, Vincent C, et al. 2008. Instruments and methods glaciological and volumetric mass-balance measurements: Error analysis over 51 years for Glacier de Sarennes, French Alps. Journal of Glaciology, 54(186): 522–532.

Ulaby F T, Moore R K, Fung A K. 1986. Microwave Remote Sensing Active and Passive Volume III: from Theory to Applications. Norwood: Artech House, 22(5): 1223–1227.

Wang N, He J, Pu J, et al. 2010. Variations in equilibrium line altitude of the Qiyi Glacier, Qilian Mountains, over the past 50 years (SCI). Chinese Science Bulletin, 55(33): 3810–3817. (in Chinese)

Wang P, Li Z, Wang W, et al. 2013. Changes of six selected glaciers in the Tomor region, Tian Shan, Central Asia, over the past ~50 years, using high-resolution remote sensing images and field surveying. Quaternary International, 311(17): 123–131.

Wang P, Li Z Q, Li H L, et al. 2020. Glaciers in Xinjiang, China: Past changes and current status. Water, 12(9): 2367.

Wang Z C, Chen Y N. 1989. Glacial geology and geomorphology in Shaksgam Valley. Arid Land Geography, 12(4): 26–31. (in Chinese)

Wu K P, Liu S Y, Jiang Z L, et al. 2019. Glacier mass balance over the central Nyainqentanglha Range during recent decades derived from remote-sensing data. Journal of Glaciology, 65(251): 422–439.

Xu A, Yang T, Wang C, et al. 2016. Variation of glaciers in the Shaksgam River Basin, Karakoram Mountains during 1978–2015. Progress in Geography, 35(7): 878–888. (in Chinese)

Yao T D, Xu B Q, Yu W S, et al. 2012. Different glacier status with atmospheric circulations in Tibetan Plateau and surroundings. Nature Climate Change, 2(9): 663–667.

Ye Q, Bolch T, Naruse R, et al. 2015. Glacier mass changes in Rongbuk catchment on Mt. Qomolangma from 1974 to 2006 based on topographic maps and ALOS PRISM data. Journal of Hydrology, 530: 273–280.

Zhang Z, Liu S Y, Wei J F, et al. 2016. Mass change of glaciers in Muztag Ata–Kongur Tagh, eastern Pamir, China from 1971/76 to 2013/14 as derived from remote sensing data. PLoS ONE, 11(1): e0147327, doi: 10.1371/journal.pone.0147327.

Zhou Y S, Li Z W, Li J. 2017. Slight glacier mass loss in the Karakoram region during the 1970s to 2000 revealed by KH-9 images and SRTM DEM. Journal of Glaciology, 63(238): 331–342.

Zyl J J V. 2001. The Shuttle Radar Topography Mission (SRTM): A breakthrough in remote sensing of topography. Acta Astronautica, 48(5–12): 559–565.